Biochimica et Biophysica Acta, 1147 (1993) 89–104

BBAMEM 75895

Tension-stabilized pores in giant vesicles: determination of pore size and pore line tension

Doncho V. Zhelev [1] and David Needham

Department of Mechanical Engineering and Materials Science, and the Center for Biochemical Engineering, Duke University, Durham, NC (USA)

(Received 24 August 1992)

Key words: Liposome; Electroporation; Pore size; Line tension

We present the first observations of giant, long-existing, stabilized pores in vesicle membranes. Using a new experimental technique for studying the electropermeabilization of lipid membranes, giant liposomes (from 25 to 56 μm in diameter) were subjected to single, square, electric pulses (duration 150 μs and electric field strength from 63 to 126 kV/m). The liposomes were held by a micropipet and small membrane tensions were created by controlling the pipet suction pressure. The liposomes were loaded with media having different refractive index from the outside solution, and, under these conditions, the formation of pores in the pressurized liposome could be visualized by the jet of inside solution that flowed out from the membrane pore. By adjusting the membrane tension, pores were kept open, and pore lifetimes could be varied from tenths of a second to several seconds. The pore size was determined from the volumetric flow in the pore region and the measured pressure differences across the bilayer. It was clear from the experiments that only one pore remained opened after the pulse. The estimated pore radii were on the order of one micrometer. The pores were in a quasi-stationary state and when they closed they did so spontaneously in a quick process (in milliseconds). The isotropic membrane tension was determined for the same measurements and from determinations of both pore size and dynamic membrane tension the pore line tension was found. The line tension of the pore region was determined for two lipid compositions, stearoyloleoylphosphatidylcholine and stearoyloleoylphosphatidylcholine with 50 mol% cholesterol, and the obtained values for single bilayers were $(0.92 \pm 0.07) \cdot 10^{-11}$ N and $(3.05 \pm 0.12) \cdot 10^{-11}$ N, respectively.

Introduction

The application of strong electric fields across a cell or lipid bilayer results in the formation and expansion of membrane pores. This process is a useful tool in cellular and molecular biology and gene technology because it allows access to cellular contents for relatively short times [1–4]. Although the direct cause of pore formation is not completely understood, a number of experimental and theoretical investigations indicate that the pores are more hydrophilic than hydrophobic, i.e., they appear to be bounded by lipid headgroups rather than exposed hydrocarbon chains. Two major theoretical approaches attempt to explain hydrophilic pore formation [2–5]. In order to help distinguish between these models it is necessary to characterize membrane breakdown in terms of the material properties of the membranes and to derive energetic models of pore formation, existence and closure.

Following pioneering studies that showed the essential features of the electroporation of cell membranes [6,7] (for review, see Zimmermann [8]), cell electroporation has become a widely used method in cellular biotechnology. Through model experiments using black lipid membranes (BLM), typical membrane characteristics such as specific conductance and capacitance have been measured. Based on these measurements, conditions have been established that optimized cell electroporation and electrofusion [9,10]. Thus, the overall phenomenology of the process of pore formation has been characterized in model membranes and the analogy between model membrane and cell membrane electrical breakdown has been shown [11], in this case with BLMs as the model system.

However, with regard to model systems, there are important differences between black lipid membranes and closed membranes (such as cell or liposome mem-

Correspondence to: D. Needham, Department of Mechanical Engineering and Materials Science, and the Center for Biochemical Engineering, Duke University, Durham, NC 27708, USA.

[1] Permanent address: Central Laboratory of Biophysics, Bulgarian Academy of Sciences, Sofia 1113, Bulgaria.

branes) that affect the way the electric field acts on the bilayer structure. A BLM is a free surface in which the lipid (and solvent) molecules of the bilayer are in equilibrium with the bulk lipid solution phase at the boundaries; the constituent bilayer molecules are free to move between bilayer and boundary reservoir in response to applied electrical (and other physical) forces. Also, the size of the BLM is characterized by the area of the aperture in which it is formed. Liposomes, on the other hand, are closed systems (on the time scale of experimentation) and the number of molecules that make up the liposome membrane is constant. Another major difference is that, at equilibrium, the BLM is always under tension ($\sim$ 1–2 dyne/cm, [12]) whilst the tension of a liposome membrane can range from essentially zero ($\sim 10^{-5}$ dyne/cm [13]; Needham and Winterhalter, unpublished results) for the unstressed state up to tens of dyne/cm when the membrane is stressed, depending on the maximum tensile strength that the bilayer can support [14]. This boundary tension condition is reflected by observations from electroporation experiments which show that the BLM is always destroyed when the pore radius exceeds a certain value called the critical pore radius [11, 15–18]. In the more recent studies of Needham and Hochmuth [19], the liposome membrane tension was actually controlled by micropipet suction, and the critical voltage for electropermeabilization was found to decrease as the level of membrane tension was increased; the tension was found to be proportional to the square of the membrane voltage as predicted by a simple work balance model.

Thus, the behavior of liposomes is therefore expected to represent the breakdown of the lipid portion of cell membranes more closely than BLMs. Like cell membranes, liposome membranes at zero tension are porated in the presence of electric fields and the critical voltage for membrane instability has been determined [19]. And, in contrast to BLMs, experiments with liposomes and cells showed that lipid membranes were not destroyed even when pores were formed that had dimensions bigger than the estimations of critical pore sizes from BLM experiments [4,19–22]. In addition, pore lifetime was found to be considerably larger for cell membranes than for BLMs [23,24]. Thus, tensions in the membrane, whether from solvent adsorption in BLMs or pressurization in liposomes and cells, act in concert with the electric destabilizing pulse. It appears that only in low tension states are pores stable and able to reclose.

One of the basic parameters that characterizes membrane pores is the line tension (the energy per unit length of the membrane contour at the pore edge). Estimations of pore line tension [25,26] were later verified by the experiments of Harbich and Helfrich [27] for lipid vesicles and by Chernomordik et al. [28] for BLMs. Values for this basic parameter are in the range 10^{-12} to 10^{-11} N. During our earlier electromechanical micropipet measurements [19] we found that a threshold membrane tension existed ($\sim$ 0.03 dyne/cm) below which the liposome in the suction pipet lost some volume and then resealed after a permeabilizing pulse. Post pulse volume changes could be a result of electroosmotic effects during the pulse [29], or of mechanical tension in the membrane or both. It occured to us that, with careful control over membrane tension, the tendency for the pore to close could be exactly balanced, and that the pore line tension might then be accessible to independent and direct measurement.

The objectives of this present work then were to attempt to determine the pore radius and membrane tension in the pore region that just opposed pore closure and to derive a relationship between these parameters that could give a measure of the pore line tension. We have already shown that cholesterol changes the material properties of the bilayer by dramatically influencing the elastic area expansion modulus and tensile strength [14,19], and so we have carried out our measurements using bilayers with and without 50 mol% cholesterol.

Materials and Methods

Liposome preparation

Giant liposomes (or vesicles), with diameters on the order of 25 μm to 50 μm, were selected from a liposome preparation. The liposomes were made following the procedure described elsewhere [14, 19]. Briefly, dried lipid lamellae were formed on a clean, roughened Teflon surface by evaporating the solvent from a lipid chloroform-methanol solution. The lipid layers were prehydrated at room temperature for half an hour using water vapor in a nitrogen carrier gas and rehydration was completed by swelling the lipid in a solution of sucrose (547 mosM) at $\sim$ 35°C. We used liposomes made from stearoyloleoylphosphatidylcholine (SOPC) with and without 50 mol% cholesterol (CHOL) (Avanti Polar Lipids, AL). After overnight incubation, the liposomes formed a loose hydrated 'cloud' in the sucrose solution. A small amount of the cloud was transferred into iso-osmotic glucose solution (558 mosM), containing 0.1% albumin. The images of the liposomes in our interference contrast microscope were thereby enhanced due to the difference in optical refractive index of the inside and outside medium. Also, the density difference between the two solutions collected the liposomes on the bottom of the microchamber for ease of capture. Solution viscosities and conductivities at 24°C were measured to be: sucrose = 1.5 mPa s and glucose = 1.27 mPa s; sucrose 113 = mS/m and glucose = 114 mS/m.

Micropipets and electro-microchamber

Micropipets with the desired geometry were made by vertical pipet puller from 1 mm diameter glass tubes and the tip was cut to the desired diameter using a microforge. The pipet entrance was filled with the same glucose solution as the solution used for suspending the liposomes, and the rest of the pipet was backfilled with iso-osmotic PBS solution. The working chamber and the pipet were grounded to prevent any possible influence of destabilizing electrostatic effects.

The experimental chamber (see Fig. 1) was made from Plexiglass and the top and bottom were covered with coverslips. The two platinum electrodes were positioned on the bottom of the chamber and were formed to create a region with a homogeneous electric field. The distance between the electrodes was 250 μm for the SOPC experiments and 300 μm for the SOPC/CHOL experiments. The square-shaped parallel region of the electrodes had a width of 1 mm. For electrical permeabilization, we used an in-house-built pulse generator (capacitance discharge, with high decay constant, where the the pulse width was controlled by an electronic switch). This arrangement gave almost rectangular pulses detected by a Tektronix storage oscilloscope. The liposomes were observed using a Leitz inverted microscope with demodulation Hofmann optics (Modulation Optics, Greenvale, NY), which is a form of interference contrast, and experiments were recorded on video. Micropipet suction pressure was measured by differential pressure transducers (Validyne, Engineering, Northridge, CA) and an indicator pulse that was synchronized with the DC pulse for electroporation were recorded along with the experimental images by video multiplexing (Vista Electronics, 8226 Vista Dr. La Mesa, CA). Subsequent analysis of the recorded experiments were carried out using video calipers (Vista Electronics, CA).

In order to calibrate pressure gradients during flow into the pipet we used small latex beads (Polystyrene microsphere with diameter 2.91 μm and standard deviation 0.068 μm, Polyscience). The flow of the beads under low suction pressures were determined in the same glucose solution as used in the experiments with liposomes. The beads were almost neutrally-buoyant in this media.

Experimental protocol

A small sample of the resuspended liposomes in glucose solution was added to the electro-microchamber at room temperature (24°C). Primary attention was given to choosing single-walled liposomes as indicated by transparency and lack of internal membranes. However, as we show in the results section some double walled liposomes were also tested. The suction pressure in the micropipet was 'zeroed' by finding the stationary, no-flow, position for a small liposome (having a diameter less than the pipet diameter).

To begin the experiment, a suitable liposome was chosen and was aspirated with a small pressure ($\sim$ 100 dyne/cm^2). The pipet and liposome were then posi-

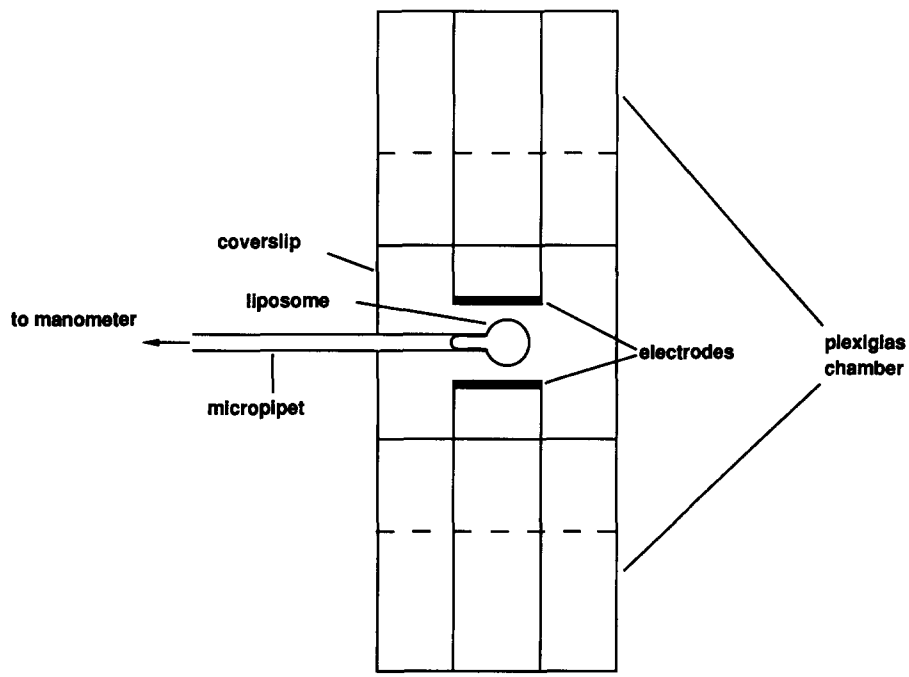

Fig. 1. Top view of the experimental chamber. The liposome (not drawn to scale) is manipulated in an open-to-the-air chamber with a micropipet held in a micromanipulator. The pipet is connected to the manometer, and the pressure difference between the pipet entrance and the manometer is measured. The vertically positioned square plane electrodes are much bigger than the liposome. The liposomes are observed with interference optics in an inverted microscope.

tioned at the middle plane between the electrodes. The desired pulse, with chosen amplitude and pulse duration, was applied. The pulse was chosen such that the liposome permeabilized even at zero membrane tension. If the liposome did not flow into the pipet, the pipet suction pressure was increased with the step of 20 dyne/cm^2 and the same voltage was applied again. This procedure was repeated until the liposome membrane started to flow inside the pipet.

Three different types of behavior were observed depending on the voltage and tension levels when the membrane was destabilized. (1) The projection length of the liposome membrane in the pipet increased after the pulse for a couple of frames (there was one frame per 1/60 of a second). (2) The liposome flowed into the pipet for a second (or seconds) and after that time stopped and the projection length remained constant. (3) The liposome flowed continuously into the pipet until the entire liposome entered the pipet. In some of the experiments, multilamellarity of liposomes was observed after the permeabilizing pulse resulting in irregular shaped secondary liposomes appearing on the outside part of the membrane. The pressure distribution in these cases could not be found from the presented model and these multilamellar liposome experiments were rejected. At the end of the experiment the pipet pressure 'zero' was checked again, and the water level difference between the 'zeroed' pipet and the level at which electroporation occurred was used to determine the pressure difference.

Micromechanical tests were also performed to check the membrane material properties (tensile strength) of the resealed liposomes. 1 min after pore sealing, the liposomes were subjected to high tension until they broke.

Results

Observation of membrane pores

The electric field strength was determined from the applied voltage and electrode geometry. The electric field in the experimental volume in which liposomes were permeabilized was assumed to be homogeneous (because the distance between the electrodes was much smaller than their characteristic length). Upon electropermeabilization of a given liposome, the region of the liposome membrane in which the pore was formed was clearly visible as shown in Fig. 2.

For permeabilization at low pipet suction pressure, the formation of a reversible pore was accompanied by a small increase of the projection length that lasted for only a few video frames (about tens of milliseconds). We did not make any quantitative estimations from the liposome volume changes in these cases, because the post-pulse volume changes were difficult to separate from the volume fluxes that may have occured during

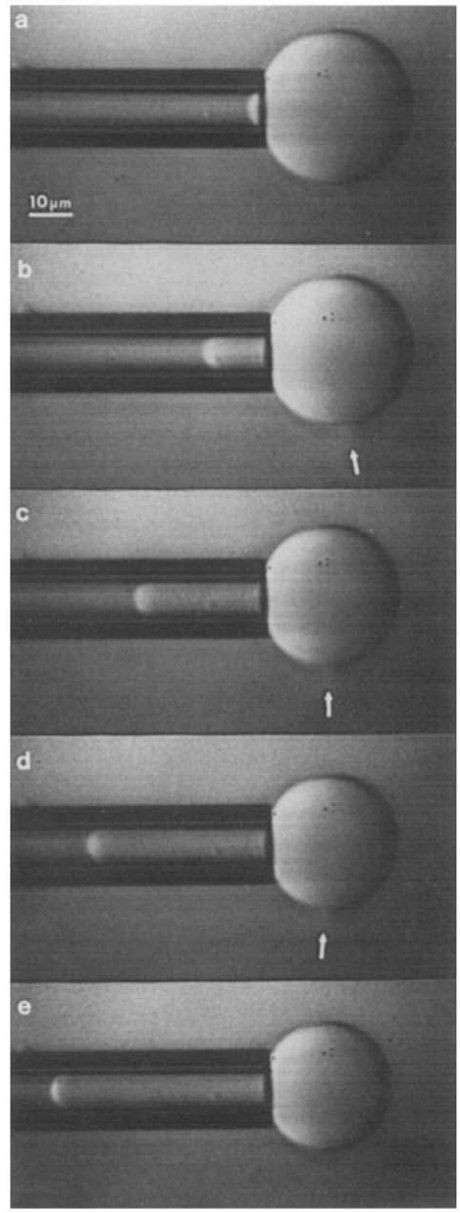

Fig. 2. Videomicrograph of liposome electroporation experiment showing the behavior of a liposome after the application of a pulse. (a) Giant liposome in the suction pipet just before pulse application. (b–d) After application of a pulse the pore forms and the liposome membrane flows into the pipet, (b) 0.5 s, (c) 1.0 s and (d) 1.5 s after the pulse. (e) The pore closed 1.7 s after the pulse and the membrane flow ceased.

the pulse (initial changes of the projection length inside the pipet can be a result of shape adjustments after the pulse).

For permeabilization at higher suction pressure, the internal media with different refractive index could be seen going out of the pore as the whole liposome moved slowly into the pipet. Conditions were attained in which reversible pores lasted from 0.3 to several seconds after the pulse was applied (an example is shown in Fig. 2) and upon pore closure, the liposome ceased its inward movement. In other cases, liposomes

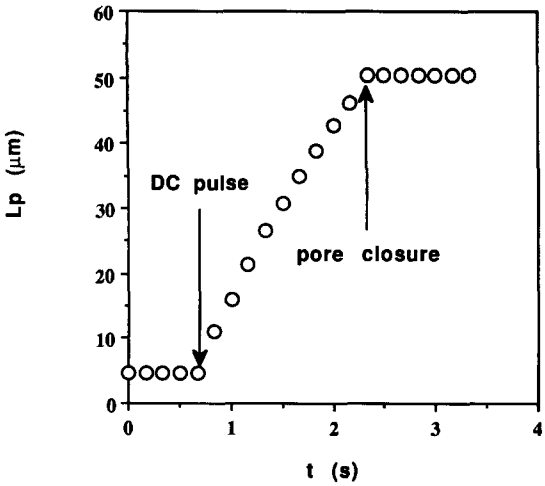

Fig. 3. Projection length L_p vs. time for a SOPC/CHOL (1:1) liposome. The first arrow indicates the moment the DC pulse was applied with duration of 150 μs and electric field strength 120.4 kV/m. The applied pressure difference between the chamber and the manometer was 5.1 Pa.

flowed completely inside the pipet as the pore did not apparently reclose. In this case, the outside part of the liposome remained spherical, the inside and outside media did not mix and the liposome maintained its different refractive index from the bathing media.

Fig. 3 shows a plot of the projection length of the liposome membrane inside the pipet vs. time for a typical experiment for SOPC/CHOL liposomes. We assumed in these experiments that the liposome area remained constant (it may be possible that some membrane area change occurred during the pulse, but this change was not measurable, i.e., less than 2%). The liposome volume was calculated for every image, and from these volumes we found the rate of volume change Q (the volume vs. time dependence was approximated by a polynomial using the least-squares method and the volumetric rate was found taking the first derivative).

Pore radius

From the volumetric flow we determined the average pore radius for the quasistationary state, assuming that the membrane around the pore does not bend and that the volume change Q represented the outgoing volume from the liposome after permeabilization and before the pore closes. The liquid volumetric flow was modelled as the flux from an orifice having radius R_{pr}, negligible wall thickness and separating two semi-infinite volumes having pressure difference ΔP. The radius of the orifice in this case and the volumetric flow Q are related by Eqn. 1 [30],

$$R_{pr}^3 = \frac{3Q\mu_i}{\Delta P} \tag{1}$$

where μ_i is viscosity of the inside fluid.

In order to calculate the pore radius from this equation the pressure difference across the pore must be estimated. We determined the pressure difference across the liposome membrane ΔP at the inside and outside caps by measuring the hydrostatic pressure difference between the chamber and the manometer, corrected for the pressure drop along the hydrostatic system,

$$\Delta P = \Delta P_m - \frac{8\mu_o(L_{eff} - L_p)V_{rt}}{R_p^2} \tag{2}$$

where, ΔP_m is the measured pressure difference, μ_o is the viscosity of the bathing medium, L_{eff} is the effective length of the pipet, L_p is the projection length of the cylindrical part of the membrane inside the pipet, and R_p is the pipet radius.

Because the applied pressure induces fluid flow, we need to define an effective length L_{eff} as the length of a cylindrical capillary having the radius R_p and the same maximum parabolic flow velocity V_{max} as the the maximum parabolic velocity in the region of observation when exposed to the same pressure difference ΔP. We characterized the effective pipet length by measuring the velocity of well defined spherical particles at the range of pressure differences as used in our experiments (see Appendix A). The effective length that we determined by this calibration was $L_{eff} = 922$ μm.

In the membrane electroporation experiments, the effective pipet length decreased with increasing projection length of the liposome membrane as the membrane flowed into the pipet. Thus, from Eqns. 1 and 2 the calculated values of pore radius for the data presented in Fig. 3. are shown in Fig. 4. It is seen that the pore radius changes about 1.5-times, decreasing almost linearly with time during a flow lasting 1.75 s.

Our estimates of pore radius upon initial permeabilization of the membrane R_{pri} and just before reclosing

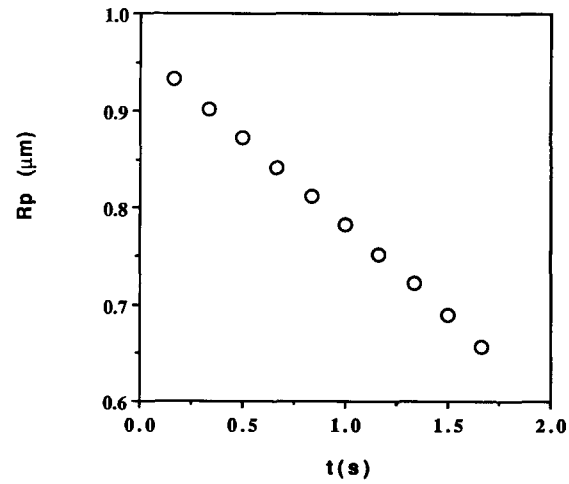

Fig. 4. Pore radius R_{pr} calculated from Eqn. 1 vs. time for the example shown in Fig. 3.

TABLE I

Initial R_{pri} and final R_{prf} pore radii, pore lifetime t_p, the outside liposome radii R_o, the membrane voltage $\Delta\varphi_m$ (V), and the static membrane tension T_{ms}, before the application of the pulse, and the electric field strength at the moment of pore formation for SOPC and SOPC/CHOL (1:1) liposomes

The pulse duration was 150 μs.

T_{ms} (mN/m)	R_o (μm)	E (kV/m)	$\Delta\varphi_m$ (V)	R_{pri} (μm)	R_{prf} (μm)	t_p (s)
SOPC						
0.028	17.2	100.0	2.58	1.66	0.65	4.5
0.033	16.5	63.3	1.57	1.26	0.71	2.8
0.042	15.6	70.0	1.64	1.28	0.93	0.25
0.042	15.5	70.0	1.63	0.84	0.60	4.8
0.030	14.7	116.7	2.57	1.10	0.68	3.2
0.065	12.2	83.3	1.52	1.23		[a]
0.040	20.3	86.7	2.64	1.75		8.9
SOPC/CHOL						
0.094	18.3	120.4	3.30	1.24		[a]
0.067	28.1	118.5	4.99	0.99	0.86	2.6
0.084	14.3	120.4	2.60	0.76		[a]
0.084	17.6	120.4	3.18	0.93	0.66	1.7
0.078	17.0	124.1	3.16	0.83	0.71	0.33
0.082	16.3	124.1	3.03	0.76	0.72	0.33
0.087	16.0	124.1	2.98	0.70	0.51	2.0
0.037	25.6	118.5	4.55	1.31		11.0
0.054	22.5	118.5	4.00	1.54		5.5
0.078	16.2	125.9	3.06	0.84	0.51	2.5

[a] Did not reseal.

R_{prf} are given in Table I for the two lipid compositions studied. In Table I we also present other mechanical and electrical characteristics of the liposome at the moment of application of the electric field (membrane tension, liposome outer radius, maximum membrane voltage), and the characteristics of the pore region after the pulse and before its spontaneous reclosing (initial and final radii of the pore and the pore lifetime). The initial and final pore radii were found from the volumetric flow rate at the moments of pore opening and closure. The time for pore reclosing was simply measured from the multiplexed time record on the video tape.

Membrane voltage $\Delta\varphi_m$

Maximum values of membrane voltage $\Delta\varphi_m$ are presented in Table I (the direction angle is equal to zero). Values for $\Delta\varphi_m$ were calculated from Eqn. 3 [31],

$$\Delta\varphi_m = -\tfrac{3}{2}ER_o\cos(\theta) \tag{3}$$

where, E is the electric field strength, is the angle between the position of a pore in the membrane and the direction of the electric field strength vector, R_o is the radius of the spherical portion of the liposome.

The membrane voltage at a given location on the membrane changes from zero (before the pulse) to the value found from Eqn. 3. The voltage increase is characterized by a decay constant [31]. In our experiments the conductivities of the inside and outside media were measured to be 113 mS/m and 114 mS/m, respectively. The specific membrane capacitance is on the order of 10 mF/m^2 and the specific membrane conductance is on the order of 10 S/m^2. Neumann [31] used the value 10 mF/m^2 for the specific membrane capacitance. For comparison, the specific conductance for black lipid membranes is of the same order of magnitude, and the specific membrane capacitance for a variety of BLM lipid compositions varies from 0.35 to 7.8 mF/m^2 [28]. Using these values, the decay constant in our experiments varies from 1.07 μs to 2.46 μs, for different size liposomes. Taking into account the pulse duration (150 μs) in our experiments, a good estimate of the maximum membrane voltage can therefore be found from Eqn. 3.

Static and dynamic membrane tensions T_{mst} and T_{osp}

Under static conditions (before permeabilization), the applied pressure goes only into creating a membrane tension and so it is straightforward to obtain the membrane tension T_{mst} as given by Eqn. 4 [32],

$$T_{mst} = \frac{\Delta P_m R_p}{2\left(1-\frac{R_p}{R_o}\right)} \tag{4}$$

where R_o is the radius of the liposome outside the pipet.

However, after permeabilization the liposome flows into the pipet and for a given applied pressure the membrane tension will be smaller than in the static case because this pressure difference is distributed between other terms. Therefore, in order to determine the membrane tension in the pore region between pore opening and closing, we require a dynamic model that takes into account how the measured pressure difference between the chamber and the manometer is distributed during liposome flow. During its existence, the pore was in a quasi-static state and, in all of the experiments, pore closure was a very fast event; it occurred between two video image frames (the time interval between frames was 1/60 s). Thus, we were able to estimate the membrane tension of the outside portion of the liposome where pore formation occurred from the corresponding pressure difference between the chamber and the control volume in our manometer system, assuming that this pressure difference was distributed between three major terms.

(1) Pressure drop inside the manometric system.

(2) Pressure drop because of the viscous drag of the liposome membrane inside the pipet; our estimation of

the viscous dissipation in the liposome membrane during membrane entry into the pipet showed that this effect was negligible, because of the small lipid membrane viscosity $(5.0–13.0) \cdot 10^{-6}$ mPa s [33].

(3) The tension of the outside liposome membrane; when there was a pore, the shape of the outside membrane portion was spherical in both, static and dynamic flow conditions. We assumed that the membrane in the outside region was subjected to isotropic tension, and we estimated its value T_{osp} (see Appendix B) by,

$$T_{osp} = \left(\frac{\Delta P_m}{2} - \frac{\mu_o V_{rt}}{R_p} \left(\frac{4(L_{eff} - L_p)}{R_p} + \frac{L_p}{h} \right) \right) \frac{1}{\left(\frac{1}{R_p} - \frac{1}{R_o} \right)} \quad (5)$$

where ΔP_m is the measured pressure difference, μ_o is the outside viscosity, V_{rt} is the measured entry velocity of the membrane hemisphere inside the pipet, R_p is the pipet radius, L_p is the projection length of the liposome membrane inside the pipet, L_{eff} is the effective pipet length, R_o is the outside liposome radius and h is the thickness of the lubricating film between the liposome membrane and the pipet wall.

All the quantities in Eqn. 5 are measurable at the time of the experiment except the effective length (L_{eff}) of the manometric system and the thickness of the lubricating film between the membrane and the pipet wall. We estimated L_{eff} from independent experiments (see Appendix A and Table A-I). The thickness of the lubricating film can vary in different experiments. An estimation of it's magnitude can be found from measuring the velocity of the trailing edge for a liposome that does not reclose as it flows into the pipet, using Eqn. B-6. For the SOPC liposome, shown in Table I, that flowed completely into the pipet, we were able to measure the length of the cylindrical portion, when the liposome was completely inside the pipet; its length was 77.3 μm, the velocity of the trailing edge was 30.4 μm/s and the pipet radius was 3.7 μm. The estimated value for the film thickness in this case was 0.1 μm. It can be seen from Eqn. 3 that the friction term is proportional to the projection length and entry velocity. In the beginning it is negligible, because the projection length is very small. We expect that the line tension does not depend on projection length (or entry velocity). We varied the estimate for the thickness of the film between from 0.1 to 0.2 μm and found that there was no distinguishable effect on the obtained values for the line tension. In all calculations we used the value 0.15 μm for the film thickness.

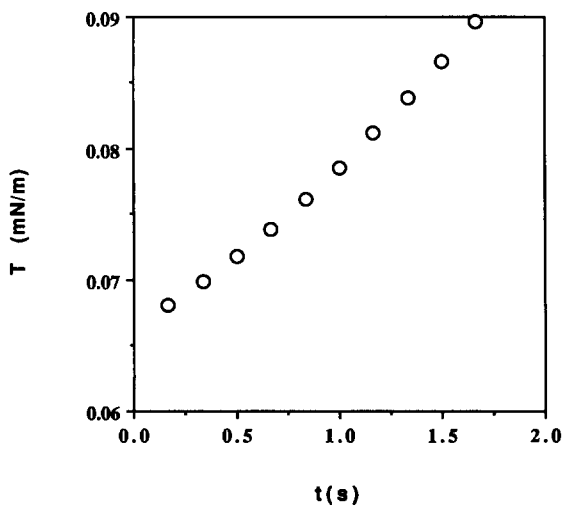

Fig. 5. Liposome membrane tension from Eqn. 7 versus time for the example shown in Fig. 3.

TABLE II

Critical membrane tension T_c for mechanical breakdown of reclosed liposomes

Lipid system	T_c (mN/m)
SOPC	1.0
	2.8
	2.3
	1.6
SOPC/CHOL	6.6
	4.0
	0.9
	2.4

Eqn. 5 gives the two limiting cases: (1) when $V_{rt} = 0$ and the liposome is in a static condition it gives Eqn. 4; (2) when $R_o = R_p$ (and $T_{osp} = 0$) it gives Eqn. B-6 for the velocity and film thickness dependence for the liposome (or any other cylindrically shaped particle), that moves inside the pipet like a plug.

Fig. 5 presents the estimated tension from Eqn. 5 for the example shown in Fig. 3. The membrane tension of the outside region increases with time until the liposome reseals or until it is completely aspirated by the pipet and the membrane tension drops to zero. When R_o is close to R_p, Eqn. 5 is very sensitive to experimental errors. In this case, it is much better to deal with the pressure drop terms, instead of membrane tension T_{osp}, and to evaluate the product $T_{osp}((1/R_p) - (1/R_o))$. In our measurements, R_o was always between two and four times bigger than R_p, and when the liposome flowed completely inside the pipet we restricted our measurements to the range where $R_o > 1.5R_p$.

Micromechanical tests were performed to check the tensile strength of the resealed liposomes. These measurements showed that SOPC liposomes broke at a smaller membrane tension compared to that for SOPC/CHOL liposomes. Also, for both compositions, all porated and resealed membranes broke at smaller tensions than their respective non-porated membranes.

The values for critical membrane tension for resealed liposomes are presented in Table II.

Discussion

Studying pores in a bilayer membranes is important for understanding the conditions under which lipid membranes can exist and are stable. We studied lipid vesicle membranes because they are the simplest closed bilayer structure. In our thermodynamic description of the pore region we take the view that, when the pore is formed, the membrane material at the pore edge can rearrange. This rearrangement would seem to involve changes in the packing of lipids from the bilayer L_α phase to packing similar to that in hexagonal phases. Then, there are three possibilities for changing the chemical potential of lipid molecules involved in the pore edge compared to the chemical potential of the same type of molecules in the planar membrane: (1) the chemical potential of a lipid molecule in the pore region can increase; (2) the chemical potential at the pore region can decrease; and (3) the chemical potential does not change. This simple qualitative presentation helps in understanding the basic conditions of membrane existence. If the number of lipid molecules in liposome membrane does not change in the time scale of the experiments, the liposome free energy can be defined as the sum of the chemical potentials of the all molecules involved. Then the liposome free energy will increase, decrease or remain constant in the three cases of chemical potential changes described above. Thermodynamically the most favorable conditions are the ones with minimum free energy. Thus, in the first case, the liposomes will exist, while in the second and the third case they will not (because every spontaneously formed pore in the membrane will increase infinitely in size and the membrane will breakdown). We define the pore line tension as the difference of the sum of the chemical potentials of lipid molecules occupying unit length of the pore edge and the sum of chemical potentials of the same number and type of lipid molecules from the planar membrane. The line tension is then the fundamental macroscopic characteristic of membrane stability. The membrane is stable only when the line tension is positive. We will now discuss the conditions that allow us to determine quantitatively this characteristic.

Pore existence

The main result from our micropipet experiments is that, once formed, the electrically induced pores can be made to exist up to 10 s after the pulse and the pore radii range in size by a factor of two. These pores closed very quickly (within two video frames) as the pore radius decreased by almost two orders of magnitude (from 0.5 μm to on the order of the membrane thickness). We assumed that the pores in these experiments were in equilibrium, and that they closed spontaneously. It was also assumed that there was only one long living pore that remained and any smaller pores closed very quickly after the pulse. The measured entry velocities in our experiments, were continuous functions of time, and we did not detect any rapid velocity changes up to the final closure. Taking into account the statistical nature of pore closure, the probability of the simultaneous closure of two or more pores in the experiments was very small. In some liposomes, there were small free liposomes encapsulated in their interior. In some instances we used these free liposomes to trace the stream lines of the fluid inside the bigger liposome, which showed that there was one pore through which it exited (see Fig. 6).

Thermodynamic considerations

At equilibrium, the isotropic membrane tension is related to the free energy of the liposome. We assumed that the force opposing any infinitesimal change of the pore radius is determined by a change of the liposome free energy. We neglected the energy necessary for rearrangement of the lipids in the membrane because of the small membrane viscosity [33] and because liquid lipid membranes do not show shear elasticity. The liposome membrane free energy in this case can be presented as a sum of the components E_{wl} and E_p [32], where the first term refers to the water–lipid interactions on both sides of the membrane, and the second term represents the interaction between the lipid molecules in the membrane, and is characterized by the lateral pressure being the result of these interactions.

$$\sigma = \left(\frac{\partial E_{wl}}{\partial \alpha}\right)$$

$$-\pi_m = \left(\frac{\partial E_p}{\partial \alpha}\right) \tag{6}$$

Thus, $\sigma/2$ characterizes changes in the free energy density at a single water-lipid boundary and π_m is the change of the lateral pressure when the unit area of the membrane changes by $\partial\alpha$.

Then, when the membrane is subjected to isotropic tension (T) at constant temperature, the work ($W(A_l)$) for an infinitesimal change of the liposome area (dA_l) is,

$$W(A_l) = \int_{A_l} T\, dA_l = \int_{A_l} (\sigma - \pi_m)\, dA_l \tag{7}$$

where A_l is the liposome area. The work $W(A_l)$, represents the change of the free energy of the liposome, when the membrane tension changes, for exam-

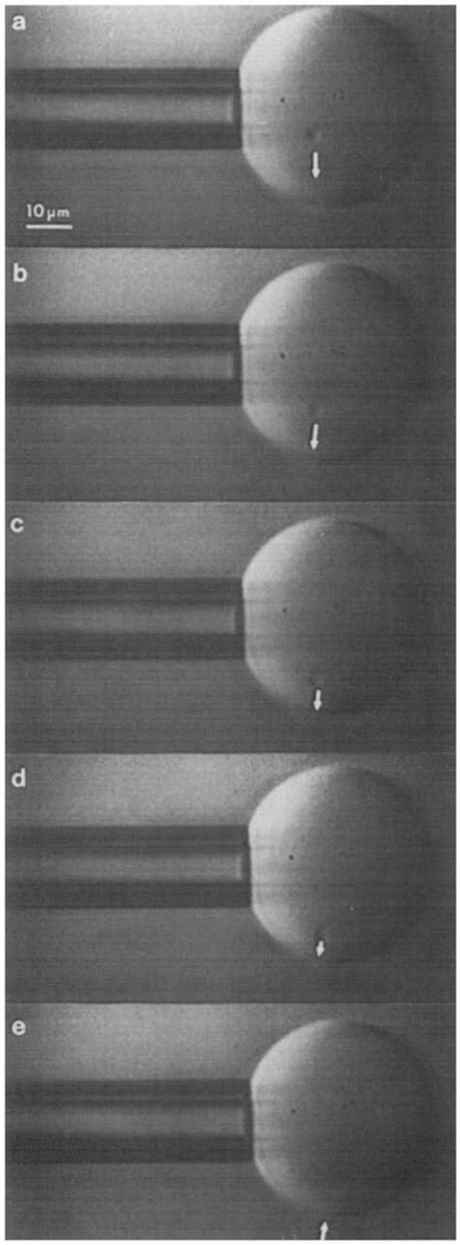

Fig. 6. Small liposome inside the large one which moves along the stream lines of the out-going fluid.

ple, as a result of changing the suction pressure in the pipet.

Now, the formation of pores in liposomes also leads to changes of their free energy. If there is one pore in the membrane, we can divide the liposome membrane into two regions: (1) pore region; (2) bilayer region (where the free energy per unit area is the same as the free energy per unit area for the closed surface subjected to the same membrane tension) as shown in Fig. 7. If the pore is stable, the energy of the pore edge should be equal to the energy of the membrane material that occupied the pore area before pore formation.

At equilibrium, the pore free energy $E_{pr}(R_{pr})$ can be defined as,

$$E_{pr}(R_{pr}) = \int_{L_p} \Gamma \, dl - \int_{A_p} T \, d\alpha = \Gamma 2\pi R_{pr} - T\pi R_{pr}^2 \quad (8)$$

where Γ is the pore line tension (energy for creating unit length at the pore edge), T is the membrane tension, R_{pr} is the pore radius, L_p is the pore perimeter, and A_p is the pore area.

Then, the force required for an infinitesimal change of the pore radius is,

$$F_p(R_{pr}) = -2\pi(\Gamma - T \cdot R_{pr}) \quad (9)$$

Our experiments showed that when the liposome was under small tension and pores were formed in the liposome membrane (e.g., by applying electric pulses), the membranes resealed very quickly; we were able to detect pore formation by the internal liquid going out of the liposome. In contrast, when the membrane tension was bigger than the tension that allowed these long-existing pores, the liposome membrane broke-down completely, the liposome deflated and was rapidly aspirated by the pipet [31]. Thus, we assumed that the long-existing pores were in a semi-stationary state and the net resultant force was zero. If this were true, the product TR_{pr} should be constant with time. It is seen from Fig. 8a,b that TR_{pr} does not change significantly with time, supporting this assumption. In Fig. 8a, the product TR_{pr} for one liposome that did not close is shown by solid circles. It is seen that, whilst the outside part of the liposome remained spherical, the product TR_{pr} increases continuously. If in this case Eqn. 5 can still apply, the pore radius is increasing. The experimental points in Fig. 8a,b for both lipid compositions are grouped into two regions and the ratio between the obtained values from the two regions is about two. We selected optically clear liposomes without any internal

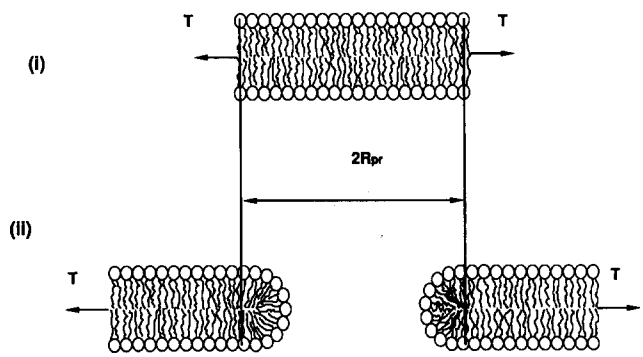

Fig. 7. Schematic of a pore in a lipid bilayer membrane that corresponds to the thermodynamic model. (i) represents molecules in an unperturbed region of membrane that has a size that is equivalent to the pore region. (ii) represents the porated bilayer showing the pore region with perturbed lipids around the edge. T signifies the direction of membrane tension and R_{pr} is the pore radius.

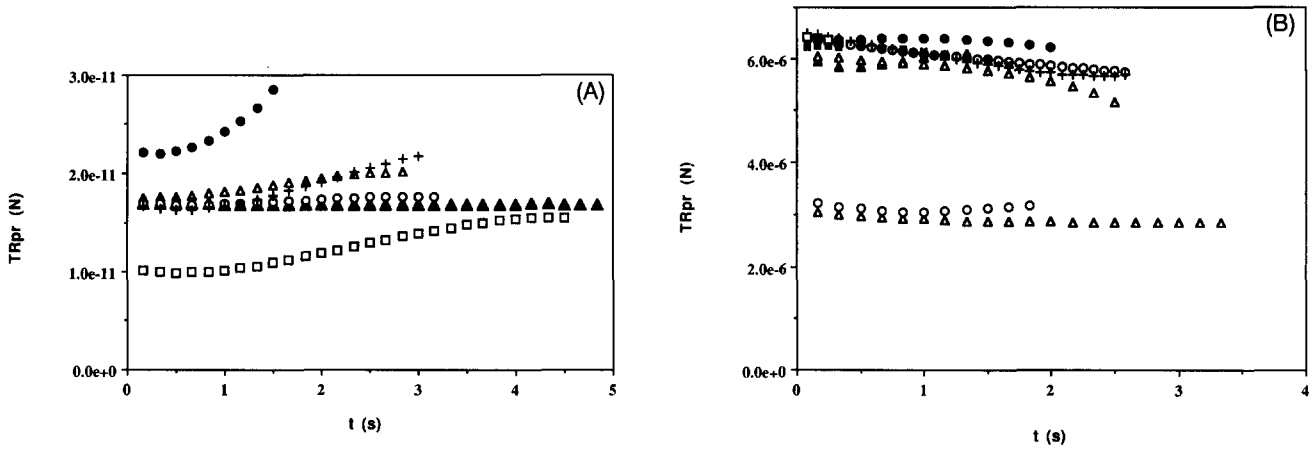

Fig. 8. The product TR_{pr} versus time for (a) SOPC and (b) SOPC/CHOL (1:1) liposomes. Different symbols represent different liposomes. The filled circles in (a) show a liposome that did not reseal.

structures in an attempt to use only single or double bilayer membranes in the micropipet test. The results show that, for these liposome preparartions, most liposomes tested contained two bilayers.

Pore line tension

To find the value for the line tension, we present the experimental data from each group in a coordinate system that does not depend on time. We chose ($1/T$ vs. R_{pr}) coordinates. The values for the pore radius found from Eqn. 1 are very sensitive to both pressure difference deviations and to the actual geometry of the pore region. We assumed that the pore was cylindrical. In this regard, Chang and Reese, using freeze-fracture electron microscopy [21] found that the majority of the pores formed by electropermeabilization in red blood cells are apparently conical in shape. The membrane bending necessary to form these conical shapes in the pore region during the pulse can be a result of electroosmotic effects [20]. If pores are in fact conical, values for the pore radius found from Eqn. 1 will be slight underestimates, and values for the membrane tension found from Eqn. 5 will be slight overestimates.

The experimental points from Fig. 8a,b are shown in Fig. 9a,b, presented in $1/T$ vs. R_{pr} coordinates. The slopes of linear regression lines to each data are estimations of the line tension. Thus the average pore line tension was determined both from the product TR_{pr} and from the slopes in Fig. 9. For the six SOPC liposomes studied, the experimental data fall into two groups. Similarly the data for the nine SOPC/CHOL liposomes fall in two groups. The line tension for the two groups for each composition were: SOPC liposomes, $1 \cdot 10^{-11}$ N and $(1.78 \pm 0.09) \cdot 10^{-11}$ N from TR_{pr} and $0.74 \cdot 10^{-11}$ N and $(1.5 \pm 0.18) \cdot 10^{-11}$ N from the slopes respectively, and SOPC/CHOL liposomes, $3.0 \cdot 10^{-11}$ N and $(6.11 \pm 0.23) \cdot 10^{-11}$ N from TR_{pr} and $3.36 \cdot 10^{-11}$ N and $(7.39 \pm 1.3) \cdot 10^{-11}$ N from the slopes, respectively. Thus, we see that, for each of the lipid compositions, the pore line tension can have one of two values. These values differ by a factor of two, and we assume that this is a result of selecting micro-

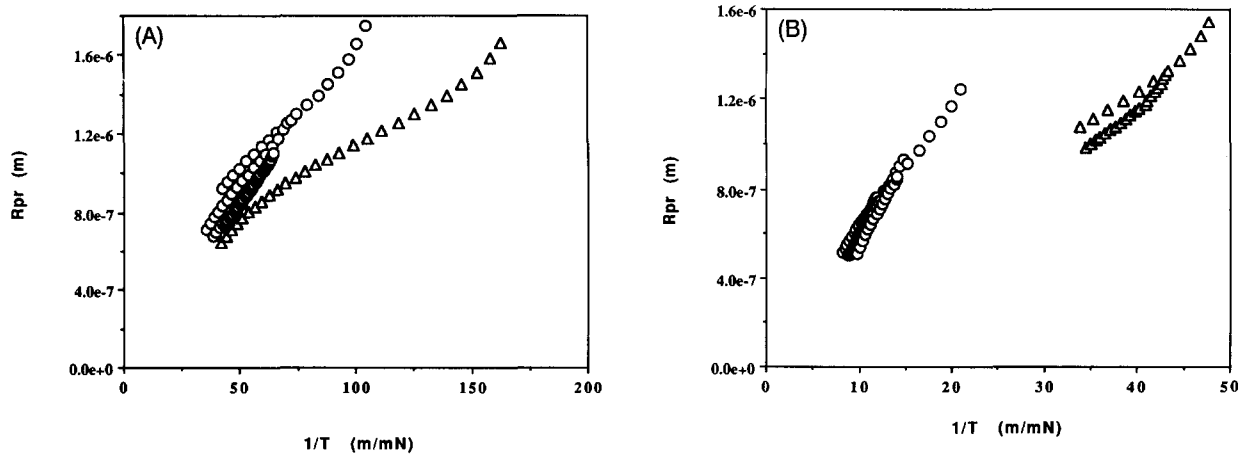

Fig. 9. Pore radius R_p versus the reciprocal far field tension T for (a) SOPC and (b) SOPC/CHOL (1:1) liposomes (the same data as in Fig. 8). Single bilayer liposomes are represented by △; double bilayer liposomes are represented by ○.

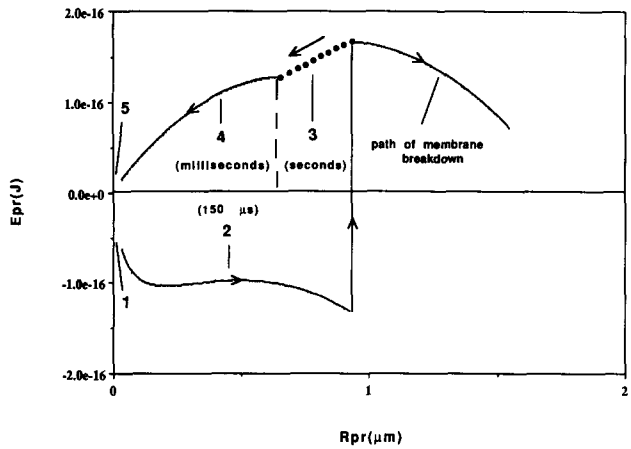

Fig. 10. Pore free energy changes during reversible pore opening and reclosure, calculated using Eqns. 13a and 13b. The arrows indicate the sequence of events, and the times for completing every stage are shown in brackets. Stages 1 and 2, pore formation and opening when a square pulse is applied (the upper boundary for the electroststic free energy is presented); stage 3, quasistationary pore, the line tension is balanced by the far-field membrane tension; stage 4, spontaneous pore reclosure; and 5, complete resealing. Also shown is a possible path for irreversible membrane failure.

scopically transparent liposomes that can nevertheless have either one or two bilayers. If we take the lowest values as representative of single bilayers then our estimations for the line tension for a single SOPC bilayer is $(0.92 \pm 0.07) \cdot 10^{-11}$ N from TR_{pr} and $(0.75 \pm 0.08) \cdot 10^{-11}$ N from the slopes; and for a single SOPC/CHOL (1:1) bilayer is $(3.05 \pm 0.12) \cdot 10^{-11}$ N and $(3.62 \pm 0.36) \cdot 10^{-11}$ N, respectively.

The values for the line tension found in both ways differ slightly, because the slopes are sensitive to deviations from linearity. We assume that the best estimations are from the product TR_{pr}, at the initial moments of membrane flow, when the projection length of the liposome membrane inside the pipet is small and the friction effects are negligible. The slopes in Fig. 9 will be affected by the thickness of the lubricating film, which is not a measurable parameter. We calculated the pore free energy from Eqn. 8 in a domain around the measured pore radius using the line tension determined in each of the two ways (see curves 3 and 4 in Fig. 10). For the line tensions found from TR_{pr} product, the pore free energy has a maximum that coincides with the pore radius that we measured, while for the line tensions determined from the slopes, in most of the cases, the extremum was shifted from this pore radius value. This is another indication that the line tension found averaging the data shown in Fig. 8 is better than that one found from the slopes in Fig. 9.

The values for the line tension found in this work are close to the value $2.1 \cdot 10^{-11}$ N, reported by Harbich and Helfrich [27] for the line tension of a PC vesicle membrane. The line tensions estimated from BLM experiments [28] for a variety of lipid compositions are of the same order, from $0.33 \cdot 10^{-11}$ N to $1.66 \cdot 10^{-11}$ N. Interestingly, the addition of lysoPC in the latter experiments lead to a decrease in the line tension. Harbich and Helfrich [27] report that the measured values of the line tension decrease when the lipid was kept for several months and the composition of the lipids possibly changed (the lipid sample was visibly darkened!!). Taken together, these results show that the line tension depends on the ability of the lipid molecules to pack at the edge region. Addition of lysoPC in BLM experiments, or the accumulation of lipid degradation products in PC vesicle experiments, favors a greater packing ability and decreases the line tension. Also, in the BLM experiments, the measured line tension is for small pore radii and in this case the measured line tension for the same lipid composition is expected to have smaller values.

In our experiments we found that the line tension increases with the addition of cholesterol and so the role of cholesterol is, most probably, to decrease the conformational freedom of the hydrocarbon region of the bilayer. This effect leads to a decrease of the effective free volume in the hydrophobic part of the membrane and restricts the packing ability (assuming constant effective volume for the lipid molecules).

Free energy of the pore region for the whole time course

In the above discussion, we have characterized the pore region in the liposome membrane *after* the pulse, deriving the formulae for the free energy of the pore region. We will now discuss the changes in the free energy of the pore region *at the beginning* and *at the end* of the pulse in order to present a complete picture of the process in terms of free energy.

The formation of a hydrophilic pore is a complex phenomenon and there are two major theoretical approaches that attempt to explain hydrophilic pore formation: (1) pores form as a result of the electric field increasing the size of pre-existing spontaneous membrane defects [9,16–18]; (2) the electric field acts preferentially on spontaneous fluctuations of membrane mechanical parameters (such as membrane elasticity or thickness) such that pores result from field-induced mechanical membrane instabilities [5,19]. From these current theories, there is as yet no universally accepted mechanism for exactly how the free energy changes in going from a planar membrane to a membrane containing a minimum sized hydrophilic pore (see Fig. 7). Although these disparate models predict an energy barrier, in the continuum approach the minimum sized defect is the hydrophilic pore itself; and in the defect models small defects evolve into the minimum hydrophilic pore but the exact geometry of the course of this evolution is not known. We believe that an energy barrier must exist for pore formation that is largely characterized by the difference in the ability of lipid

molecules to pack at the edge region compared to the planar lipid bilayer.

The dynamics of the pore region during increases in radius is also a complicated problem, and as yet little theoretical work has addressed this issue. Here, we use a thermodynamic approach to characterize the free energy changes of a hydrophilic pore as a function of the pore radius. We attempt to show a quantitative estimation of the pore free energy changes, (or in cases where this is not possible we find the limits) when the pore radius increases during the pulse and the pore closes after the pulse. This can be an example of the 'relaxation hysteresis' proposed by Neumann [31], where, instead of the electric field strength, we use the pore free energy and the structural parameter is the pore radius.

We assume that the free energy of the pore is well characterized by its size. We were not able to estimate the pore radius during formation of a hydrophillic pore and so we assume that the minimum pore radius of a hydrophilic pore is on the order of the membrane thickness. The maximum pore radius at the end of the pulse application was found from the volume flux measurements at $t = 0$. The free energy of the pore region during the pulse is:

$$E_{pr} = \Gamma 2\pi R_{pr} - T\pi R_{pr}^2 - \frac{\pi(\epsilon_w - \epsilon_l)}{h_m^2}\int_0^{R_{pr}} \frac{\Delta\varphi_{pr}^2(r) r\, dr}{\left(1 + \frac{\pi r k_p(r)}{2h_m k_e}\right)^2} \quad (10)$$

where ϵ_w and ϵ_l are water and lipid permittivities, h_m is membrane thickness, $\Delta\varphi_{pr}(r)$ is the voltage in the pore region, $k_p(r)$ and k_c are pore and bulk conductivities, respectively.

The first two terms in Eqn. 10 are the same as in Eqn. 8; the third term refers to the increase in free energy of the pore region in an external electric field due to the fact that lipids (having small dielectric constant) have been replaced by a material (aqueous solution) that has a relatively high dielectric constant. In general, the voltage in the pore region is a function of the distance from the pore rim. It is assumed in Ref. 34 that when the pore radius is much less than the vesicle radius, the pore in the vesicle has similar electrical characteristics as a pore in a BLM, where the voltage in the pore region is considered constant. This approach was successfully used [18] for modeling the dynamics of BLM instability. We think that the voltage in the pore region will depend mostly on the ratio of the pore radius to the thickness of the charged double layers on both sides of the membrane. Then, the voltage in the pore region in this case will show a time dependence, because of the double layer discharge. The problem is an interesting one in itself, and its solution should be found numerically. This is a moving boundary problem and involves seeking a solution of a system of nonlinear partial differential equations. However, there are no experimental data available for the dependence of the pore radius on the pulse length.

Another complication can arises from the fact that membrane instability in most of the cases does not go through the formation of a single pore, but it is likely that many pores are formed. The existence and/or formation of many pores can lead to a tremendous drop of the voltage in the pore. When the voltage in the pore region is chosen to be constant with time and position, and equal to the voltage of a polarized nonporated membrane $\Delta\varphi_m$, the above formula provides an upper boundary for the electrostatic free energy. We can distinguish two pore sizes: (1) small pores, pores with radii on the order of the membrane thickness; (2) big pores, when the pore size is much bigger than the electric double layer thickness for a given membrane and electrolyte solution. For small R_{pr} the conductivity of the pore region can be small compared to the bulk conductivity [15] and the membrane tension can be equated to the static membrane tension (see Table I). For big pores, the pore and bulk conductivities are equal and, the membrane tension is now that for the flowing membrane (which is less than the static tension).

Then, the free energy for small pores, when $k_p \ll k_e$ is,

$$E_{pr} = \Gamma 2\pi R_{pr} - T\pi R_{pr}^2 - \frac{\pi(\epsilon_w - \epsilon_l)\Delta\varphi_m^2 R_{pr}^2}{2h_m^2} \quad (11a)$$

and the upper limit for the free energy for big pores, when $k_p = k_e$ is,

$$E_{pr} = \Gamma 2\pi R_{pr} - T\pi R_{pr}^2 - \frac{4}{\pi}(\epsilon_w - \epsilon_l)\Delta\varphi_m^2\left(\ln\left(\frac{\pi R_{pr}}{2h_m}\right) + \frac{2h_m}{\pi R_{pr}} - 1\right) \quad (11b)$$

We can now represent the free energy as it changes with pore radius by using our measured values for line tension and pore radius and assuming the following values: 3 nm for membrane thickness of a single bilayer and 6 nm for the double bilayer, $80\epsilon_o$ and $2\epsilon_o$ for water and lipid permittivities (where ϵ_o is the permittivity of the free space–$8.8542 \cdot 10^{-12}$ ($CN^{-1}m^{-2}$)). Fig. 10 shows the free energy dependence on pore size (calculated using Eqns. 11a and 11b) for one liposome from the moment of pulse application to pore resealing. We distinguished five main stages of the pore region during this process for a reversible pore. These are: (1) formation of a hydrophilic pore; (2) increase of the pore size; (3) pore equilibrium; (4) spontaneous closing of the pore; (5) spontaneous *complete* resealing.

For ease of discussion, these stages can be conve-

niently divided into two groups. The first group consists of the first two stages, 1 (pore formation) and 2 (pore size expension) during the time period in which the external electric field is on. In this first stage we would expect a free energy barrier which corresponds to the formation of the hydrophilic pore. However, this stage is not shown in the figure, because as discussed above, it is not clear at the moment which model (continuum or defect) can be used to derive this dependence.

After formation, the hydrophilic pore will expand until the electrostatic term and the tension term are bigger than the line tension term. The membrane discharge will eventually lead to stabilising of pores or they may even start to reclose until discharging current equals the charging current from the applied external field for very long pulses. We show in Fig. 10 the upper boundary of the electrostatic free energy. In another model, in which the tangential current in the planar membrane domain close to the pore region is taken into account [35], a second extremum in the free energy does appear, and big pores are predicted to be eventually stabilized by the electric field. However, we did not use this latter model for calculating the electrostatic part of the free energy, because even if discharge effects are not taken into account it predicts smaller pore radii than what we experimentally observed.

The second group, stages 3, 4 and 5, is concerned with the time period after the pulse and so the electrostatic term in the free energy is zero. Our experiments have focused primarily on stage 3 (equilibrium stage); we have simultaneously changed the pore radius and the membrane tension. As a result, their product remained constant, which provides the equilibrium condition that allows the pore to be kept open for several seconds. If this delicate balance is not achieved the pore can follow one of two paths: it can follow the path for membrane breakdown; or it can enter stage 4. During stage 4 (spontaneous closing of the pore) the pore radius decreases spontaneously (this process is very fast), and it probably reaches the kind of values determined by the initial hydrophilic pore size. Finally in stage 5 (spontaneous complete resealing) pore completely reseals depending on the magnitude of the energy barrier for the transition from minimum size hydrophilic pore to planar membrane (not shown in Fig. 10 for the same reasons as for those in stage 1). Interestingly, our measured values for critical membrane tensions of resealed liposomes (Table II) are smaller than the average tension for failure of nonporated liposomes. This result suggests that although pores reclosed they also did not reseal completely, up to 1 min after closure. Conductance measurements with BLMs also show that such small, 'closed' pores can in fact remain open from several seconds to minutes [15].

This temporal behavior of pores in lipid membranes contrasts strongly with the existence of long living pores in cell membranes [23,24,36,37]. The length of time that cell membrane pores can exist extends from minutes up to several hours. Thus, when compared to the lifetime of the small pores in lipid bilayers, it would appear that diffusion of lipids in cell membranes does not limit closing rather, the redistribution of lipid and protein components at the pore edge can dramatically reduce the line tension. Pore resealing may then be more a function of the ability of the cell to repair the membrane defects [38].

In conclusion, this paper presents the first observations of giant, long-living metastable pores in liposome membranes. Our mechanical characterization of this state has allowed us to determine the line tension of the pore region for SOPC and SOPC/CHOL (1:1) bilayers, which are very close to the values obtained by Harbich and Helfrich [27] for a PC vesicle membrane and Chernomordik et al. [28] for BLMs. It is shown that for an unstressed lipid bilayer membrane there is no critical radius for breakdown, and that such a membrane tends to form a spontaneously closed surface (this condition is valid when the composition of the edge region remains the same as the surrounding planar part of the membrane). It follows from this that an unattached sheet of lipid bilayer will always tend to form a closed vesicle.

Appendix A. Calculation of effective pipet length, L_{eff}

Table A-I shows the results from our experiments for the calibration of the manometric system. L_{eff} is the effective pipet length, ΔP_{cor} is the additional pressure drop on the spherical particle, and V_{max} is the maximum velocity of the Poiseuille flow. The measurements were made for different suction pressures in order to cover the range of values for V_{max} in our liposome experiments. From Table A-I we see that the additional pressure drop, because of the presence of a particle, is small compared to the total pressure drop. Thus, in our calibration experiments for estimating L_{eff} the presence of the particle did not affect the pressure distribution along the pipet and the latter can be safely estimated using Eqn. 2.

The estimated values for the effective pipet length using latex beads and liposomes are similar. The advantage of using small particles is that their velocities are better predicted by the theoretical models than larger particles. However, the small particle velocity is more sensitive to positional deviations from the axis of symmetry. The estimated values from the latex beads calibration are bigger than the values from liposome measurements. There is a small trend of the estimated values for L_{eff} with total pressure drop ΔP in both measurements. In our calculations we used the mean

TABLE A-I

Effective pipet length L_{eff}, determined from velocity measurements of latex particles and small liposomes for different suction pressures ΔP

D_{sphere} is the particle diameter, V_{max} is the velocity at the pipet axes, ΔP_b is the pressure drop correction factor, because of the presence of the particle, L_{eff} is the effective pipet length.

ΔP (Pa)	D_{sphere} (μm)	V_{max} (μm/s)	L_{eff} (μm)	ΔP_b (mPa)
Latex beads				
10	2.9	32.5	829	3.4
10	2.9	34.1	790	3.5
10	2.9	33.8	796	3.5
10	2.9	30.5	884	3.1
10	2.9	34.0	793	3.5
10	2.9	33.7	800	3.5
20	2.9	65.9	818	6.8
20	2.9	47.6	1133	4.9
20	2.9	66.4	811	6.9
20	2.9	54.7	986	5.6
20	2.9	49.3	1092	5.1
20	2.9	55.1	978	5.6
30	2.9	71.1	1137	7.3
30	2.9	72.6	1113	7.5
30	2.9	71.5	1131	7.4
30	2.9	77.2	1048	8.0
Liposomes				
10	5.6	30.3	891	20.6
10	6.1	32.5	829	34.0
10	5.8	29.8	905	24.2
15	6.2	47.7	847	54.1
15	4.4	42.8	945	8.7
20	6.0	68.4	788	65.8
20	5.3	58.9	915	30.5
20	4.9	55.5	971	19.4
20	5.7	61.5	877	45.8
25	5.6	71.0	949	48.4
25	6.1	74.3	907	77.7
25	5.0	72.6	929	28.1
25	6.2	79.3	849	89.9

value for L_{eff} from all experiments. Thus the effective length that we determined by this calibration was $L_{eff} = 922$ μm.

We used small spherical latex beads in our experiments for pipet calibration, and tracked their flow into the pipet for different pressures. For simplicity we choose the beads that remained in an axial position in the pipet. The problem of particle flow into a cylinder is widely studied. Hochmuth and Sutera [39] showed that there is good agreement between experimental observations and theoretical predictions for small (below 0.6) and high (above 0.8) ratios of particle to pipet radii. For small ratios the dominating effect was the additional pressure drop, because of a presence of the particle, while for big ratios the dominating was the effect of friction with the wall.

The maximum velocity of the Poiseuille flow V_{max} was found from the measured beads velocities V_b, from the condition for the total force acting on the particle. In our case the pipet was positioned horizontally and the gravity field was perpendicular to the pressure gradient, and even big deviations from buoyancy would not affect the force acting on the particle, but can change its position. The total force F along the axis is [30,40],

$$F = -6\pi\mu_o R_b(K_1 V_b - K_2 V_{max}) \tag{A-1}$$

where R_b is the latex bead radius, μ_o is the viscosity of the suspending media, and the constants K_1 and K_2 are [41],

$$K_1 = \frac{1 - 0.75857\lambda^5}{1 - 2.105\lambda + 2.0865\lambda^3 - 1.7068\lambda^5 + 0.72603\lambda^6}$$

where, $\lambda = R_b/R_p$ and,

$$K_2 = \frac{1 - \frac{2}{3}\lambda^2 - 0.20217\lambda^5}{1 - 2.1050\lambda + 2.0865\lambda^3 - 1.7068\lambda^5 + 0.72603\lambda^6}$$

From the force balance on the sphere $F = 0$, we estimated the maximum velocity V_{max} for the Poiseuille flow inside the pipet.

$$V_{max} = \frac{K_1}{K_2} V_b \tag{A-2}$$

The additional pressure drop in particle region was estimated by Eqn. A-3 [40],

$$\Delta P_b = \frac{8\mu_o V_{max}}{R_b}\lambda^5 \tag{A-3}$$

For determination of the maximum velocity of the Poiseuille flow we used also small liposomes. The small liposomes could be considered as neutrally buoyant deformable particles. The liquid drop would not deform if [42,43],

$$\frac{\mu_o V_{max}\lambda^2}{\gamma} \ll 1 \tag{A-4}$$

where γ is the interfacial tension.

In our preparation most of the liposomes were multilamellar. Their resistance for deformation depends both, on the bending stiffness (bending modulus for a single bilayer multiplied by the number of layers) and on the inside and outside osmotic pressure difference. In our experimental conditions the liposomes behave as rigid particles.

Appendix B. Estimate of membrane tension T_{osp} during liposome flow

Typical measured velocities were around 30 μm/s, the fluids were water solutions and with density close

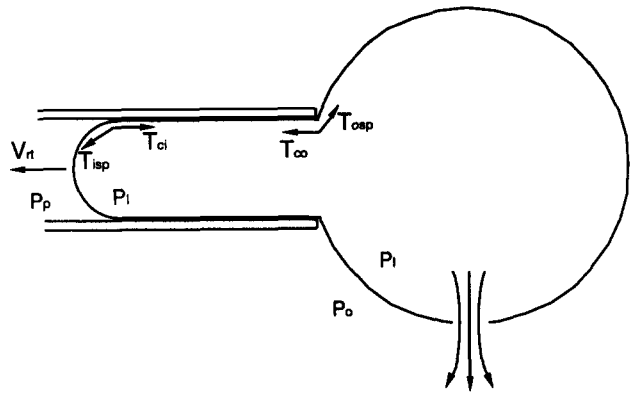

Fig. B-1. Schematic illustration of a liposome with a pore moving into a cylindrical pipet with a velocity of the leading edge V_{rt}. The pressure in the pipet is P_p, in the liposome is P_l, and the pressure in the chamber is P_o. Different regions of the liposome membrane are subjected to different tensions. The membrane tension at the leading spherical cap is T_{isp}, the tension in the cylindrical section decreases from T_{ci} inside the pipet to T_{co} at the pipet orifice, and the far field tension of the outside spherical section is T_{osp}. The tensions are balanced at the boundaries of the adjacent regions.

to water density, the characteristic sizes of moving boundaries were approx. 10 μm, and the viscosity of the media were close to water viscosity, 1 mPa s. This values gave a Reynolds number of $\sim 10^{-4}$. Thus, our experiments were performed at low Reynold numbers, and we could neglect inertial effects. The sketch of the problem is shown in Fig. B-1. As, shown, we recognized three geometric regions: (1) the hemispherical cap inside the pipet, (2) the cylindrical membrane section inside the pipet, and (3) the spherical shaped outside part.

We assumed that the velocity distribution of the liquid inside the pipet and far from the liposome membrane was 'Poiseuilleous', while the liquid velocity in the liposome in the first and second regions was constant (plug flow). For the liquid velocity of the outside region at the inside and outside of the membrane we assumed that it was a continuous function, and, since the inside and outside viscosities were almost equal, we neglected the velocity term in the balance of forces at the membrane.

The membrane tension in the inside hemisphere T_{isp} could be found from the Laplace formula,

$$T_{isp} = \frac{R_p(P_l - P_p)}{2} \tag{B-1}$$

where R_p is the pipet radius, P_p is the static pressure in the pipet, P_l is the static pressure in the liposome.

Similarly the isotropic membrane tension of the outside membrane could be estimated by,

$$T_{osp} = \frac{R_o(P_l - P_o)}{2} \tag{B-2}$$

where R_o is the radius of the outside spherical sector.

The membrane tension along the cylindrical shaped membrane is increasing from the pipet orifice to the hemispherical cap, because of the viscous drag along the pipet wall. We assumed that there was a thin lubricating film between the pipet wall and the liposome membrane with thickness h. It was assumed that, for the low tensions created during membrane entry, the membrane area remained constant. Thus, the velocity of the membrane along the axis would be equal for all of the points of the membrane in this region and it would be equal to the velocity of membrane entry V_{rt}. Then, if the membrane tension at the inside end of the cylindrical part is T_{ci}, and at the pipet orifice is T_{co}, there is a relationship between them, (taking into account the drag along the pipet wall),

$$T_{co} = T_{ci} - L_p \frac{\mu_o V_{rt}}{h R_p} \tag{B-3}$$

where μ_o is the viscosity of the outside liquid, L_p is the projection length of the cylindrical region inside the pipet.

The membrane tensions at the boundaries between every two of the three regions are equal,

$$T_{isp} = T_{ci}, \quad \text{and} \quad T_{osp} = T_{co} \tag{B-4}$$

Then, from Eqns. B-1 to B-4, the isotropic membrane tension of the outside portion of the liposome membrane can easily be found,

$$T_{osp} = \left(\frac{\Delta P}{2} - \frac{L_p m_o V_{rt}}{R_p h}\right) \frac{1}{\left(\frac{1}{R_p} - \frac{1}{R_o}\right)} \tag{B-5}$$

where ΔP is the pressure difference outside the membrane leading edge and the experimental chamber (the static pressure in the experimental chamber is in order of magnitude of the atmospheric pressure).

The thickness of the lubricating film can be found from measuring the velocity of the trailing edge of the liposomes which did not seal and were completely aspirated into the pipet.

$$h = \frac{2 L_c R_p \mu_o V_{rt}}{R_p^2 \Delta P - 8 \mu_o (L_{eff} - L_c) V_{rt}} \tag{B-6}$$

where L_c is the length of the cylindrical section of the liposome.

Acknowledgements

This work is supported by grant GM 40162 from the National Institutes of Health. David Needham is grateful to the Alfred M. Hunt Fund for the Hunt Faculty Scholarship Award.

References

1 Dimitrov, D.S. and Jain, R.K. (1984) Biochim. Biophys. Acta 779, 437–468.
2 Zimmermann, U. (1986) Rev. Physiol. Biochem. Pharmacol. 105, 175–256.
3 Neumann, E., Sowers, A.E. and Jordan, C.A. (1989) Electroporation and electrofusion in cell biology, Plenum Press, Ney York, NY.
4 Tsong, T.Y. (1990) Bioelectrochem. Bioenerg. 24, 271–295.
5 Dimitrov, D.S., Zhelev, D.V. and Jain, R.K. (1985) J. Theor. Biol. 113, 353–377.
6 Kinosita, K. and Tsong, T.Y. (1977) Biochim. Biophys. Acta 471, 227–242.
7 Kinosita, K. and Tsong, T.Y. (1979) Biochim. Biophys. Acta 554, 479–497.
8 Zimmermann, U. (1982) Biochim. Biophys. Acta 694, 227–277.
9 Abidor, I., Arakelian, V., Chernomordik, L., Chizmadzhev, Y.A., Pastushenko, V. and Tarasevich, M. (1979) Bioelectrochem. Bioenerg. 6, 37–52.
10 Benz, R. and Zimmermann, U. (1980) Biochim. Biophys. Acta 640, 169–178.
11 Chernomordik, L., Sukharev, S., Popov, S., Pastushenko, V., Sokirko, A., Abidor, I.G. and Chizmadzhev, Y.A. (1987) Biochim. Biophys. Acta 902, 360–373.
12 Needham, D. and Haydon, D.A. (1983) Biophys. J. 41, 251–257.
13 Evans, E. and Rawicz, W. (1990) Phys. Rev. Lett. 64, 2094–2097.
14 Needham, D. and Nunn, R. (1990) Biophys. J. 58, 997–1009.
15 Chernomordik, L.V., Sukharev, S.I., Abidor, I.G. and Chizmadzhev, Y.A. (1983) Biochim. Biophys. Acta 736, 203–213.
16 Kashchiev, D. and Exerova, D. (1983) Biochim Biophys. Acta 732, 133–145.
17 Sugar, I.P. and Neumann, E. (1984) Biophys. Chem. 19, 211–225.
18 Barnett, A. and Weaver, J.C. (1991) Bioelectrochem. Bioenerg. 25, 163–182.
19 Needham, D. and Hochmuth, R.M. (1989) Biophys. J. 55, 1001–1009.
20 Dimitrov, D.S. and Sowers, A.E. (1990) Biochemistry. 29, 8337–8344.
21 Chang, D.C. and Reese, T.S. (1990) Biophys. J. 58, 1–12.
22 Kinosita, K., Hibino, M., Hiroyasu, I., Shigemori, M., Hirano, K., Kirino, Y. and Hayakawa, T. (1992) in Guide to electroporation and electrofusion (Chang, D.C., Chassy, B.M., Saunders, J.A. and Sowers, A.E., eds.), pp. 29–46, Academic Press, San Diego, CA.
23 Saulis, G., Vensalauskas, M.S. and Naktinis, J. (1991) Bioelectrochem. Bioenerg. 26, 1–13.
24 Lopez, A., Rols, M.P. and Teissié, J. (1988) Biochemistry. 27, 1222–1228.
25 Taupin, C., Dvolaitzky, M. and Sauterey, C. (1975) Biochemistry. 14, 4771–4775.
26 Lister, J.D. (1975) Phys. Lett. 53A, 193–194.
27 Harbich, W. and Helfrich, W. (1979) Z. Naturforsch. 34a, 1063–1065.
28 Chernomordik, L.V., Kozlov, M.M., Melikyan, G.B., Abidor, I.G., Markin, V.S. and Chizmadzhev, Y.A. (1985) Biochim. Biophys. Acta 812, 643–655.
29 Dimitrov, D.S. and Sowers, A.E. (1990) Biochim. Biophys. Acta 1022, 381–392.
30 Happel, J. and Brenner, H. (1986) Low Reynolds number hydrodynamics, p. 258, Martinus Nijhoff, Dordrecht.
31 Neumann, E. (1989) in Electroporation and electrofusion in cell biology (Neumann, E., Sowers, A.E. and Jordan, C.A., eds.), pp. 61–82, Plenum Press, New York.
32 Evans, E.A. and Skalak, R. (1980) Mechanics and Thermodynamic of Biomembranes, CRC Press, Engelwood Cliffs, NJ.
33 Waugh, R.E. (1982) Biophys. J. 38, 29–37.
34 Pastushenko, V.F. and Chizmadzhev, Y.A. (1983) Biofizika (in Russian) 28, 1036–1040.
35 Winterhalter, M. and Helfrich, W. (1987) Phys. Rev. A. 36, 5874–5876.
36 Sowers, A.E. and Lieber, M.R. (1986) FEBS Lett. 205, 179–184.
37 Teissié, J. and Rolls, M. (1986) Biochem. Biophys. Res. Commun. 140, 258–266.
38 Zhelev, D.V. and Needham, D. (1992) in Biologic Effects of Electric and Magnetic Fields (Carpenter, D.O., ed.), Academic Press, Orlando, FL.
39 Hochmuth, R.M. and Sutera, S. (1970) Chem. Eng. Sci. 25, 593–604.
40 Brenner, H. (1970) J. Fluid Mech. 43, 641–660.
41 Haberman, W.L. and Sayre, R.M. (1958) David Taylor model basin, Report No. 1143, Navy Dept., Washington, DC.
42 Hetsroni, G., Haber, S. and Wacholder, E. (1970) J. Fluid Mech. 41, 689–705.
43 Brenner, H. (1971) Ind. Eng. Chem. Fundam. 10, 537–543.